Atmospheric Pollution Research 10 (2019) 1267–1275

HOSTED BY

Contents lists available at ScienceDirect

Atmospheric Pollution Research

journal homepage: www.elsevier.com/locate/apr

Original research article

# Exploring the stratospheric source of ozone pollution over China during the 2016 Group of Twenty summit

Zhi-Zhen Ni[a], Kun Luo[a,*], Xiang Gao[a], Yang Gao[b], Jian-Ren Fan[a], Joshua S. Fu[c], Chang-Hong Chen[d]

[a] State Key Laboratory of Clean Energy, Department of Energy Engineering, Zhejiang University, Hangzhou, 310027, China
[b] Key Laboratory of Marine Environment and Ecology, Ministry of Education of China, Ocean University of China, Qingdao, 266100, China
[c] Civil & Environmental Engineering, The University of Tennessee, Neyland, UK
[d] Shanghai Academy of Environmental Sciences, Shanghai, 200233, China

ARTICLE INFO

*Keywords:*
Ozone pollution
Stratospheric intrusion
Tropopause fold
WRF-Chem
Extratropical cyclogenesis

ABSTRACT

The 2016 Group of Twenty (G20) Hangzhou Summit was concurrently accompanied by extratropical cyclogenesis. To investigate whether the extratropical cyclone exerts any impact on the near surface ozone concentration, the Weather Research Forecast with Chemistry (WRF-Chem) model, with stratospheric passive tracers turned on, was used to simulate the air quality from August 24 to September 06, 2016. It turns out the WRF-Chem model generally performed well when compared to the observed data from a large number of air quality monitoring sites and satellite measurements. During the period, an occurrence of stratospheric intrusion was observed, associated with tropopause fold and curved upper-level jet in East Asia. A fairly large number of stratospheric passive tracers that had quite positive correlation with $O_3$ concentrations were also found over the southeast China. Besides, observed ground surface anomaly of high $O_3$ and the accompanied low CO as well as humidity further implied the downward transport of $O_3$ from the stratosphere. These results suggest that stratospheric ozone intrusion acts as an additional source of the near surface tropospheric ozone concentration, which deteriorates the $O_3$ pollution in China. This helps to explain the difficulty of $O_3$ control during the campaign period of the G20, and provides some insights into stratosphere-to-troposphere transport of $O_3$.

## 1. Introduction

Tropospheric ozone ($O_3$) plays a critical role in oxidation and regulates the lifetime of chemically and climatically relevant trace gases in the atmosphere. As a primary component of photochemical smog, $O_3$ pollution threatens human health (Kheirbek et al., 2013) and vegetation (Landry et al., 2013), ranking the third-most damaging greenhouse gas (Monks et al., 2015). Severe $O_3$ pollution events have occurred in many countries and have become a global concern during the past decades (Calfapietra et al., 2016; Lelieveld et al., 2009; Wang et al., 2017).

Although tropospheric $O_3$ is primarily a secondary product resulting from the photochemical reactions under anthropogenic and natural precursors (Xie et al., 2014; Xue et al., 2014, 2016), the anthropogenic emission control efforts may fail to reduce $O_3$ concentrations in many parts of the world (Royal Society, 2008) as downward transport from the stratosphere may be considered as another important source of tropospheric $O_3$ (Boothe and Homeyer, 2017). This downward transport is referred to as the stratosphere-to-troposphere transport (STT) or the stratospheric intrusion (Greenslade et al., 2017). The STT can be induced by deep overshooting convection, tropical/extratropical cyclones and mid-latitude synoptic-scale disturbances (Frey et al., 2015; Shankar Das et al., 2016; Stohl et al., 2003). The stratospheric $O_3$ intrusions undergo long-range transport and mixing, with up to half of the ozone diffusing within 12 h following descent from the upper troposphere (Trickl et al., 2014). Historical investigation of 15,978 extratropical cyclones in the northern hemisphere shows that stratospheric $O_3$ intrusions occur in southwest of the cyclone center, coinciding with a lowered tropopause and enhanced potential vorticity (Jaeglé et al., 2017). Besides, the vertical cyclone circulations with internal updrafts and peripheral downdrafts also have an extremely strong effect on $O_3$ redistribution (Fadnavis et al., 2011; Shu et al., 2016).

Peer review under responsibility of Turkish National Committee for Air Pollution Research and Control.

* Corresponding author. State Key Laboratory of Clean Energy Utilization, Institute for Thermal Power Engineering of Zhejiang University, NO. 38 Zheda Road, Hangzhou, 310027, China.
*E-mail address:* zjulk@zju.edu.cn (K. Luo).

https://doi.org/10.1016/j.apr.2019.02.010
Received 31 October 2018; Received in revised form 17 February 2019; Accepted 17 February 2019
Available online 20 February 2019

The STT affects the tropospheric $O_3$ budget and may impact ambient air quality if transported to the planetary boundary layer (Fiore et al., 2002). Although the anthropogenic emissions usually play dominant role at the ground level, significantly increased surface $O_3$ levels due to the STT have been observed in the United States (Lefohn et al., 2011; Lin et al., 2015), the Middle East (Lelieveld et al., 2009), the Greenland (Helmig et al., 2007) and the eastern Mediterranean (Akritidis et al., 2016). Associating with the subtropical upper-level jets, frequent STT events have also been observed in the western China (i.e., Mount Waliguan) during summer (Ding and Wang, 2006) and other regions of Asian like the Himalayas (Ojha et al., 2017; Sarangi et al., 2014). However, the STT events vary with the strength, weather pattern, topography, and season. In China, although considerable research efforts have been devoted to the near-surface chemical $O_3$ generation and the reductions of anthropogenic precursor emissions, the upper-air STT impacts on the tropospheric $O_3$ pollution, particularly in East China, has not been sufficiently investigated (Wang et al., 2017).

This paper aims to explore the stratospheric source of $O_3$ pollution in China during the campaign period of the 2016 G20 Summit (August 24–September 6, 2016). During this period, stringent short-term emission control measures seem to take no immediate effect on $O_3$ pollution (Su et al., 2017). Because of severe concerns regarding $O_3$ concentrations and the summer cyclonic weather pattern, the aforementioned pollution control event attracted wide policy-related interest. In the present study, the Weather Research Forecast with Chemistry (WRF-Chem) model that has been evaluated and applied extensively in the scientific community (Baklanov et al., 2014; Powers et al., 2017), was used to simulate the large-scale atmospheric environment during the campaign period. The rest of this paper is organized as follows. Section 2 outlines the modeling methodology, and Section 3 delves into the evolution of $O_3$ and its tagged tracers from model results, surface measurements and satellite retrievals. Finally, a summary of the findings is presented Section 4.

## 2. Methods

### 2.1. The modeling system

The WRF-Chem model is a regional online coupled chemical transport model that simultaneously simulates chemical and meteorological components by using identical physical schemes, grid structures, and transport schemes (Grell et al., 2005). In this study, two-way nested model domains were designed, namely an outer domain 1 (horizontal resolution: 75 km) covering East Asia and an inner domain (horizontal resolution: 25 km) covering eastern China, with a “Lambert conformal conic” projection, as shown in Fig. 1(a). The domains comprised default WRF-Chem vertical layers with 35 terrain-followed sigma pressure layers overall and model top at 50 hPa. By using two-way nesting, we performed simulations from August 10 to September 6, 2016, during which the period of August 24–September 6, 2016 has been analyzed to avoid the influence of the model spin up during the first few days. The model physics and chemistry schemes were listed in Table S1 of the supplementary material. Similar modeling settings have been successfully applied in our previous study (Ni et al., 2018).

The geographical data (i.e., terrain elevations, soil properties, and albedo) were primarily derived from the United States Geological Survey database (Brown et al., 1993). The meteorological boundary and initial conditions were sourced from the final operational global analysis (FNL; $1^\circ \times 1^\circ$ grid spacing) data of the National Centers for Environmental Prediction (http://rda.ucar.edu/datasets/ds083.2/). To reduce the meteorological deviations during the integration (Stauffer et al., 1991), analysis nudging was applied to temperature (T), zonal (U) and meridional wind (V) and water vapor (Q), with the nudging coefficient of $3 \times 10^{-4}$ $s^{-1}$ for T, U, V and $1 \times 10^{-5}$ $s^{-1}$ for Q. The chemical lateral boundary and initial conditions were retrieved from the results of the global Model for Ozone and Related Chemical Tracers Version 4 (MOZART4) (Emmons et al., 2010). To include a representation of stratospheric chemistry, an upper boundary condition for chemical species were specified by climatological data (www2.acom.ucar.edu/wrf-chem).

The anthropogenic emissions were obtained from the Multi-resolution Emission Inventory for China (http://www.meicmodel.org/) (Li et al., 2017a, b). The sector-based emission inventories were formatted into hourly model-ready emissions by applying temporal profiles based on the previous study (Wang et al., 2011). Moreover, the anthropogenic emissions were adjusted based on the actual implementation policy during the campaign period of G20 submit on several sectors (http://dqhj.mep.gov.cn/qyxtyzwrhjyd/), with details shown in Table S2. In addition to the anthropogenic emissions, the biogenic emissions were estimated using the Model of Emission of Gases and Aerosols from Nature (Guenther et al., 2006).

### 2.2. Model evaluation method

To ensure the credibility of the interpretation of the model's results, the model's performance was first evaluated based on the observed and modeled results. In this study, the modeled $O_3$ concentrations were compared with the surface observational data from 1011 air quality monitoring sites (blue dots in Fig. 1(b)). These observational $O_3$ data were mostly measured with a UV photometric analyzer (Thermo Scientific, Model 49i) with a detection limit of 0.5 ppb and a precision of 1 ppb (Li et al., 2017a, b). The calculated statistical indicators included the Pearson's correlation coefficient (R), the mean fractional bias (MFB), and the mean fractional error (MFE), with formula shown in

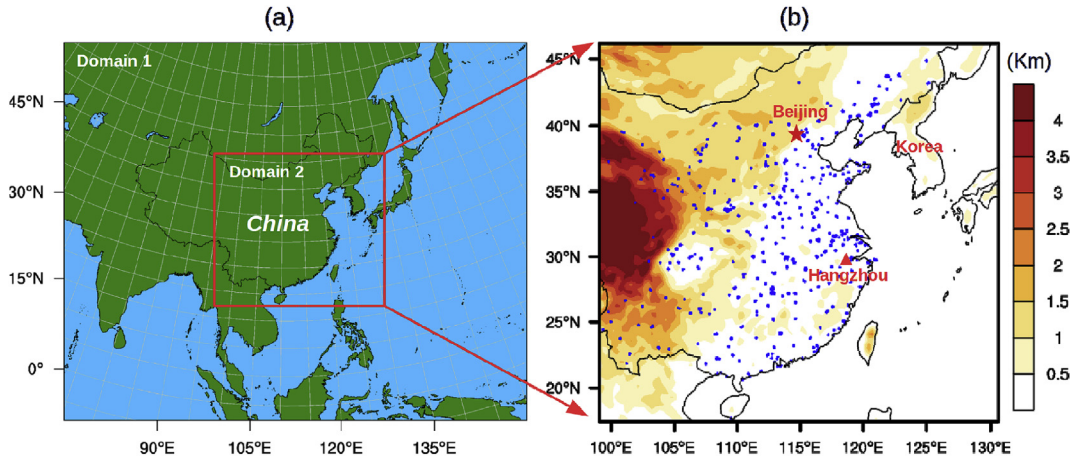


**Fig. 1.** (a) Model domains with 75-km and 25-km nested resolutions. (b) 1011 air quality monitoring sites (blue points) and terrain heights (shaded) in China.

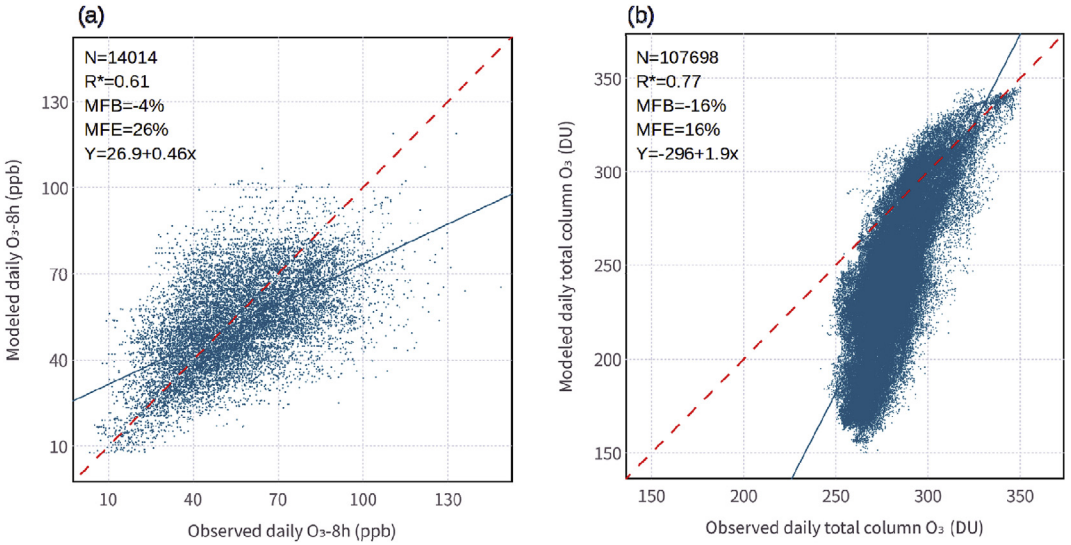


**Fig. 2.** Comparison and linear regression (confidence interval 95%) of the modeled $O_3$ against (a) the measurements at 1011 air quality monitoring sites, and (b) the OMI satellite retrievals in 12,312 horizontal domain-grids during August 24–September 6, 2016.

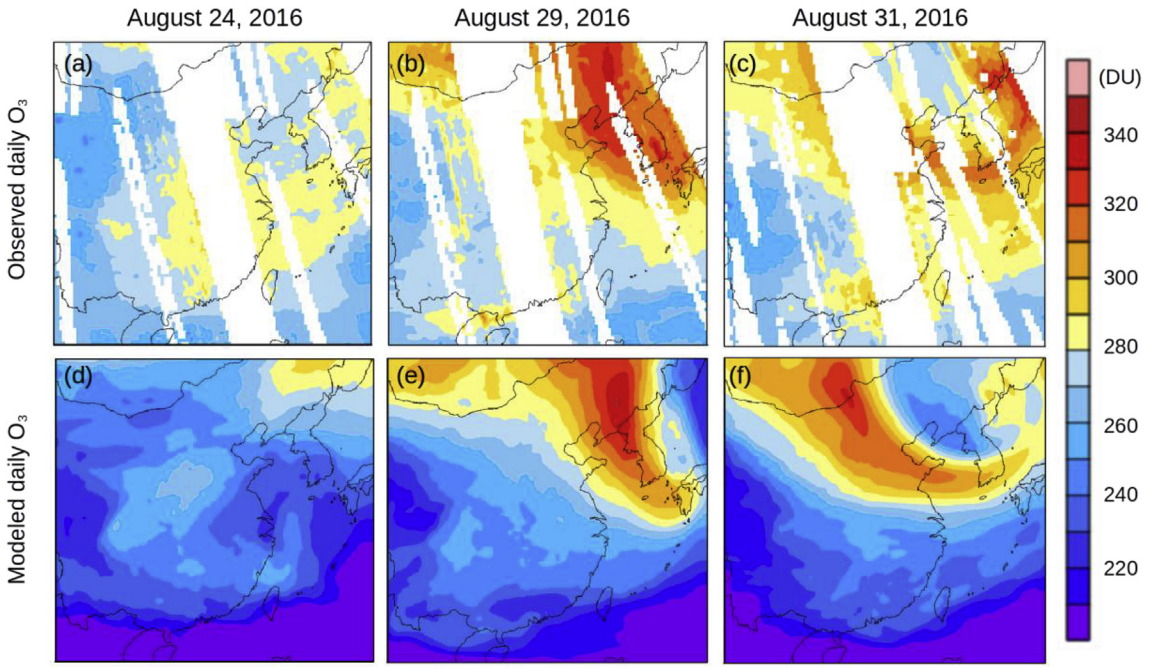


**Fig. 3.** Spatial distribution comparisons of the daily total column $O_3$ from (a–c) the satellite retrievals and (d–f) the WRF-Chem modeling on typical pollution days. The narrower swaths (white blank) are the missing measurements.

Table S3, as recommended by US Environmental Protection Agency (U.S.EPA, 2007) for $O_3$ to filter extreme fluctuations. These metrics could be used as less stringent criteria at low concentrations to account for the higher uncertainties near the detection limits.

In addition to the surface observations, satellite data of Ozone Monitoring Instrument (OMI) were used to further evaluate the modeling results. The OMI is a wide-angle, non-scanning and nadir-viewing instrument aboard the EOS Aura spacecraft measuring the solar backscattered irradiance in a swath of 2600 km. In the present study, the OMI Level 3 daily global product "OMTO3e" was downloaded from https://mirador.gsfc.nasa.gov. This product was processed by using the best pixel data over small equal angle grids (0.25 × 0.25°) covering the whole globe. The total column ozone, the radiative cloud fraction, and the solar and viewing zenith angles were included from approximate 15 orbits. More details about the algorithm and data quality have been discussed by OMI team (2012). In order to quantitatively compare the OMI satellite data and the WRF-Chem model results, the OMI data were linearly interpolated to the model grid (25 × 25 km).

### 2.3. Tracer tagging method

A tracer tagging method was used to diagnose contributions of stratospheric sources to tropospheric $O_3$. Tracers representing stratospheric air are referred as stratospheric tracers. In the WRF-Chem model, the stratospheric tracers are equally set to a value of 1 above the tropopause. This means that the tracers have a continual source and are not mass conserved. Considering as completely passive, the stratospheric tracers, accounting for tagged $O_3$ at the stratosphere within the model domain, are physically transported during the WRF-Chem simulations. Correlations between the passive stratospheric tracers and

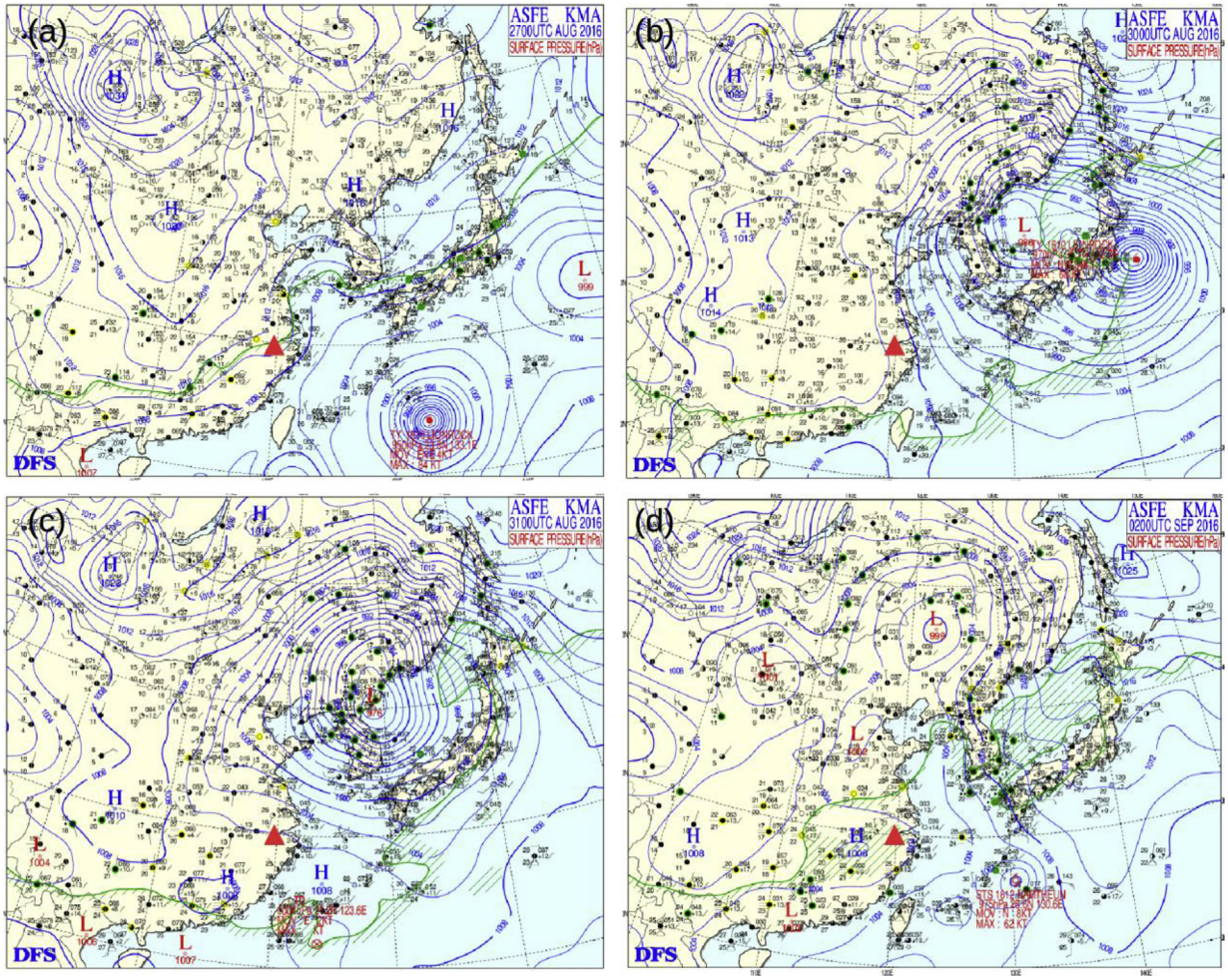


**Fig. 4.** Observed extratropical cyclogenesis in East Asia. Surface weather charts for four representative periods at 08:00 LST on (a) August 27, (b) August 30, (c) August 31, and (d) September 2, 2016. LST: Local Sidereal Time; H: High-pressure system; L: Low-pressure system. Red triangle denotes the location of Hangzhou.

the $O_3$ concentration can be used to qualitatively determine the contributions from the stratosphere, as recommended by Barth et al. (2012).

To investigate the upper-level weather systems and the evolution of synoptic-scale flow, the potential vorticity (PV) perspective was used to analyze the features of the tropopause. The tropopause has a crucial structure that divides the high PV stratosphere and the low PV troposphere (Hoskins, 2015). A PV surface such as PV = 2 PVU ($10^{-6}$ $m^2$ K $s^{-1}$ $kg^{-1}$) is referred to as a dynamical tropopause at the midlatitude (Morgan and Nielsen-Gammon, 1998). The PV diagnostics can be used as markers of the STT processes: elevated tropospheric $O_3$ and PV indicate that the downward transport from the upper troposphere and the lower stratosphere (Holton et al., 1995).

## 3. Results and discussions

### 3.1. Model performance evaluation

The daily maximum 8-h average $O_3$ concentration ($O_3$-8h) and the total $O_3$ column calculated from the WRF-Chem model output were compared with measurements at the surface air quality monitoring sites and the satellite retrievals. An r-test ($\alpha = 0.05$) was performed to test the statistical significance and 95% confidence level was achieved for the correlations. The model-simulated $O_3$ levels were in reasonable agreement with the observations during the study period, as indicated by the statistically significant correlations in Fig. 2. Fig. 2(a) shows that the modeled $O_3$-8h levels agreed well with the monitoring data with a statistically significant correlation of $R^* = 0.61$. The averaged MFB of −4% and MFE of 26% over the 1011 monitoring sites were all within the benchmarks (MFB: 15% and MFE: 35%) according to the US Environmental Protection Agency (U. S. EPA, 2007). These performances are comparable to a few previous studies (Tuccella et al., 2012; Zhang et al., 2016).

In addition to the surface measurements, the OMI satellite retrievals were also used for evaluating the model performance. Fig. 2(b) shows that the modeling system was able to reasonably reproduce the daily measurements of the total $O_3$ column, showing a statistically significant correlation of $R^* = 0.77$ compared with the satellite retrievals. The mean MFB and mean MFE of the total column $O_3$ were −16%, 16%, respectively. However, it is noticeable that an underestimation of the total column $O_3$ appeared according to the regression line. Such underestimation was partly related to the unconsidered upper-air emission sources such as the lightning-induced NOx (Schumann and Huntrieser, 2007) and the aircraft-induced NOx (Gauss et al., 2006), which contribute to $O_3$ perturbations aloft. In addition, the difference in vertical layers between the model and the OMI is of course another important factor of the evaluation bias. However, such comparison still has value as the OMI total ozone products can be effective in detecting tropospheric ozone variations (Yang et al., 2010). It should be noted that albeit of the bias, the current modeling system performed excellently for the higher value region (> 300 DU) of the total column $O_3$, which is the major concern of the present study. As an example, Fig. 3 shows the spatial distribution comparisons of the daily total column $O_3$ between the satellite retrievals and the WRF-Chem modeling results on typical

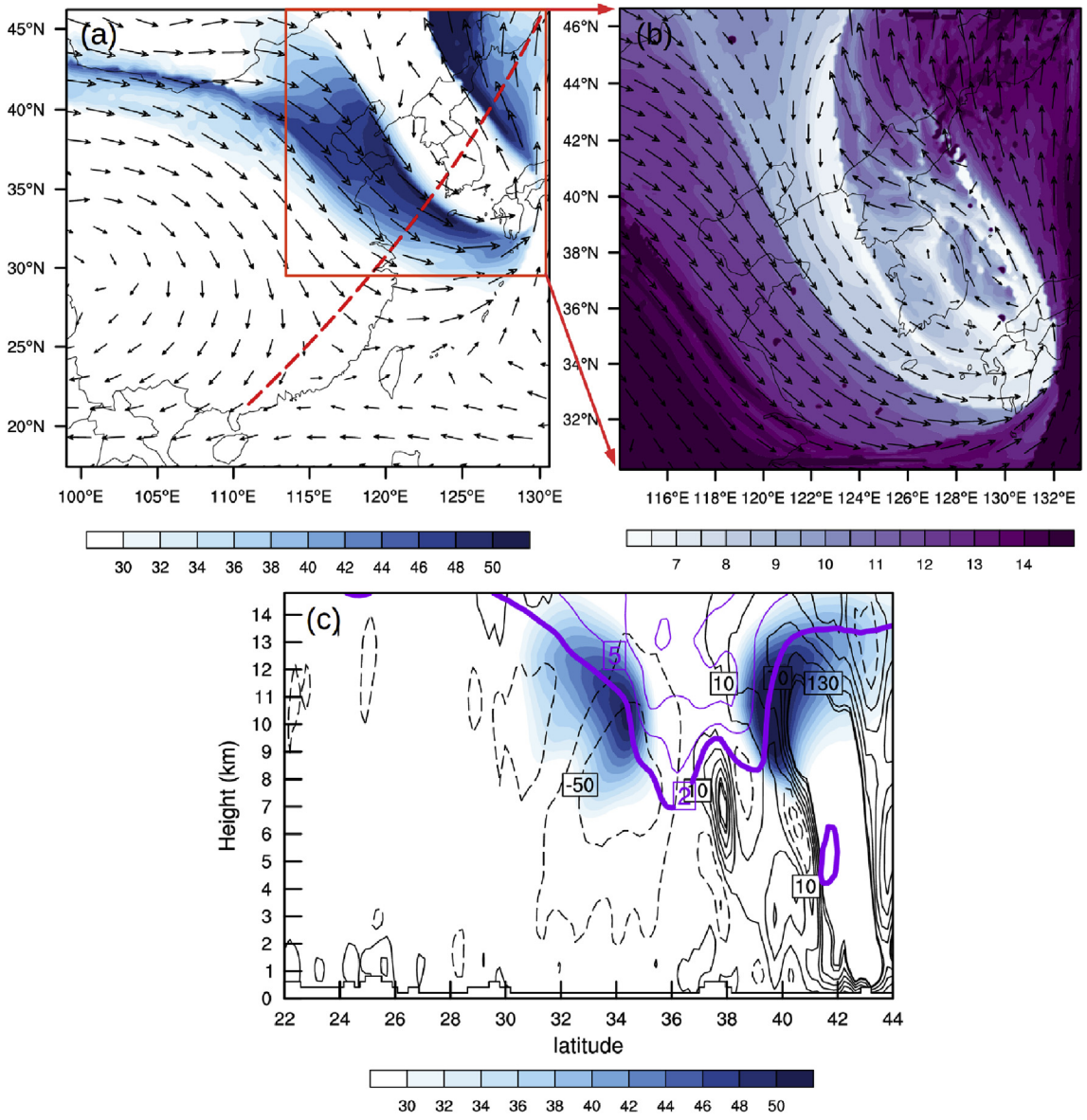


**Fig. 5.** Modeled dynamical tropopause surface (PV = 2 PVU) for (a) wind (vectors) and wind speed (shaded, m $s^{-1}$), (b) potential height (shaded, km), (c) vertical cross-section (along the red dashed line in Fig. 5(a)) of PV (purple isolines, PVU), wind speed (shaded, m $s^{-1}$), vertical wind velocity (contour, interval 30 mm $s^{-1}$) over East Asia at 2:00 LST, August 29, 2016. The dynamic tropopause marks the PV transition (thick purple line).

pollution days. It is clear that the model was able to capture well the severe $O_3$ pollution event on August 29, 2016 over the northern part of eastern China and the Korean peninsula, as expected. All these evaluations indicate that the current WRF-Chem simulations are able to reasonably reproduce the ozone concentrations at both the ground level and the upper-air level.

### 3.2. Synoptic weather patterns

Fig. 4 shows the four representative surface weather charts obtained from the Korea Meteorological Administration (http://www.kma.go.kr) which were used to track the specific cyclogenesis in the East China Sea. During August 24–28, 2016, a tropical cyclone moved northeastward in the East China Sea, and the subtropical high-pressure fields covered the vast regions of the eastern China, as shown in Fig. 4(a) in which only the chart for 8:00 LST on August 27 is presented for clarity. On August 30, 2016 (Fig. 4(b)), an extratropical low-pressure system, namely the extratropical cyclone, formed over the eastern Japan, accompanied by long and narrow cold-frontal and warm-frontal precipitation bands. Thereafter, the organized extratropical cyclone moved toward the northeastern China (close to North Korea) and affected the eastern China with a

Considerable convergent radius on August 31, 2016, as shown in Fig. 4(c). This extratropical cyclone nearly faded on September 2, 2016 (Fig. 4(d)). Meanwhile, the subtropical high recovered gradually and large-scale precipitation over the southeastern China arose in the following days. These weather charts confirm the appearance of the cyclonic weather during the study period.

Diagnostic quantities for the synoptic weather system on a typical day of the extratropical cyclogenesis predicted by the current WRF-Chem model are shown in Fig. 5. The time of 2:00 LST was selected to exclude the impact from the photochemical reactions. An upper-level jet stream was defined as a minimum wind speed in excess of 30 m $s^{-1}$ (Fig. 5(a), (c)). It can be seen that along the tropopause surface, the upper-level jets were positioned westward and downward toward the extratropical cyclone, appearing cyclonically at a high-level curvature near the Korea regions (or southern Japan). The tropopause fold was identified by the decreased potential heights on the tropopause map as

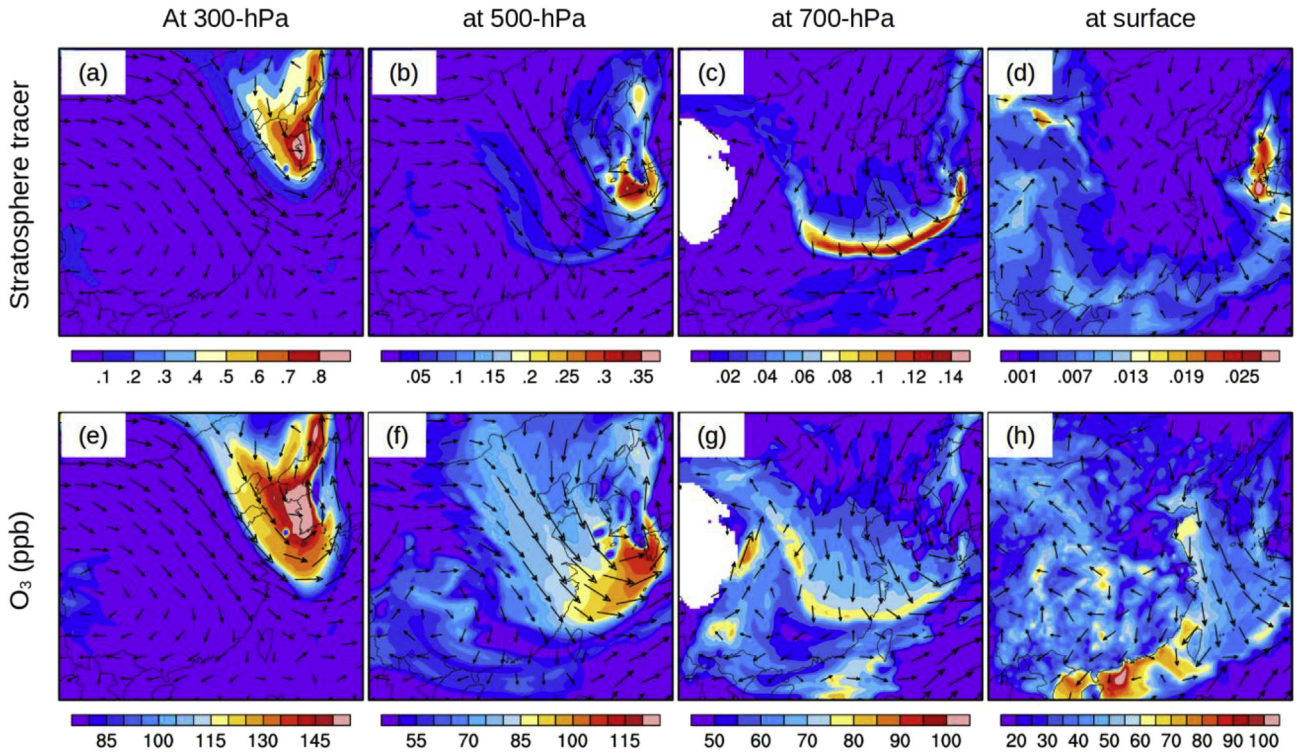


**Fig. 6.** Modeled distributions of the stratospheric tracers, the $O_3$ concentration (ppb) and the wind fields (vectors) in China, at different pressure levels at 2:00 LST on August 29, 2016. (At the stratosphere, the passive tracer is set to a value of 1).

shown in Fig. 5(b) and a downward curvilinear dynamical tropopause PV contour (PV = 2 PVU) on the cross-section as shown in Fig. 5(c). The folded tropopause was divided into the high PV stratosphere above and the low PV troposphere below. The high PV gradients coincided with the upper-level jet at the tropopause level, which was referred to as the large positive PV anomalies. Progressively thicker layers of the stratosphere were also observed to be drawn to the tropopause fold. Besides, the tendency of the vertical motion was found to ascend to the east and descend to the west. As a result, the instantaneous downward vertical wind velocity (negative dashed lines) on the western side of the folded tropopause was exceeding 50 mm $s^{-1}$.

Obviously, the stratospheric intrusion occurred during this period. Such intrusion was associated with the tropopause folds during an extra-cyclone development over the East China Sea. The tropopause folds, appearing as the curved upper-level jets during cyclogenesis in this study, were produced through cross jet geostrophic circulation favored by the associated cold advection (Keyser and Shapiro, 1986). The upper-level jet streaks may transport downward some stratospheric air directly along the descent cyclonic trajectories. The tropopause folds decreased the heights of the low stratosphere and resulted in the stratospheric air sinking to the mid-troposphere. It should be noted that the tropopause folds were always accompanied by large positive PV anomalies. In addition to amplify the extratropical cyclogenesis feedback (Bresky and Colucci, 1996), these large positive PV anomalies can produce quasi-geostrophic vertical descent motions or synoptic-scale subsidence, especially on the western side of the tropopause folds (Hoskins et al., 2003; Hoskins, 2015).

### 3.3. Impact of the stratospheric intrusion on the tropospheric $O_3$

To further investigate the possible impact of the tropopause folds on the tropospheric ozone concentration, the spatial distributions of the stratospheric tracers and the $O_3$ concentration at 2:00 LST on August 29, 2016 were shown in Fig. 6. As can be seen that the horizontal distribution patterns of the stratospheric tracers and the $O_3$ concentrations on different isobaric surfaces were similar, showing obvious positive correlations. At the high-troposphere (Fig. 6(a), (e)), high values of the stratospheric tracers, accompanied by high $O_3$ concentrations were observed in the regions of tropopause folds (over Korean Peninsula) due to the stratospheric intrusion. This is consistent with the $O_3$ satellite retrievals as shown in Fig. 3(a). The stratospheric intrusion also remarkably contributed to the mid- and the low-tropospheric $O_3$ levels (Fig. 6(b), (c), (f), (g)), with values of stratospheric tracer up to 0.35 and 0.14, respectively. Besides, stratospheric tracer with correlated high $O_3$ concentration formed a “long-narrow belt”, driven by the cyclonic wind fields. This implies that the cyclonic wrapping of the $O_3$-rich air from the stratosphere was intensely transported into the

Downwind regions such as the Southeast China. Similar to the distribution pattern in the upper air, a fairly large number of the stratospheric tracers were also observed at the ground level (Fig. 6(d)), partly explaining the nocturnal $O_3$ pollution in the southeastern and coastal China (Fig. 6(h)).

Fig. 7 shows the quantitative correlations between the simulated stratospheric tracers and the O3 concentration at 2:00 LST on August 29, 2016. As observed in Fig. 6, the simulated stratospheric tracers and the O3 concentration do have strong positive correlations. However, the correlation coefficient gradually decreases from 0.81 at the high-troposphere region to 0.33 at the ground. These evidences further confirm the observations in Fig. 6.

In addition to the horizontal distribution of the stratosphere $O_3$ intrusion evidence, a Hovmoller type diagram (height vs. time) is shown in Fig. 8, displaying the temporal evolution of ozone concentration at various heights over the site of Jingdezhen, China. Similar correlation patternsa

Were found between the stratospheric tracers and $O_3$ concentrations, particularly during the period of extratropical cyclogenesis near August 29, 2016 (dashed box in Fig. 8(a), (b)). Remarkably high values of stratospheric tracers (up to 0.2) were also observed in the mid- and low-troposphere (Fig. 8(a)), accompanied with high $O_3$ concentration

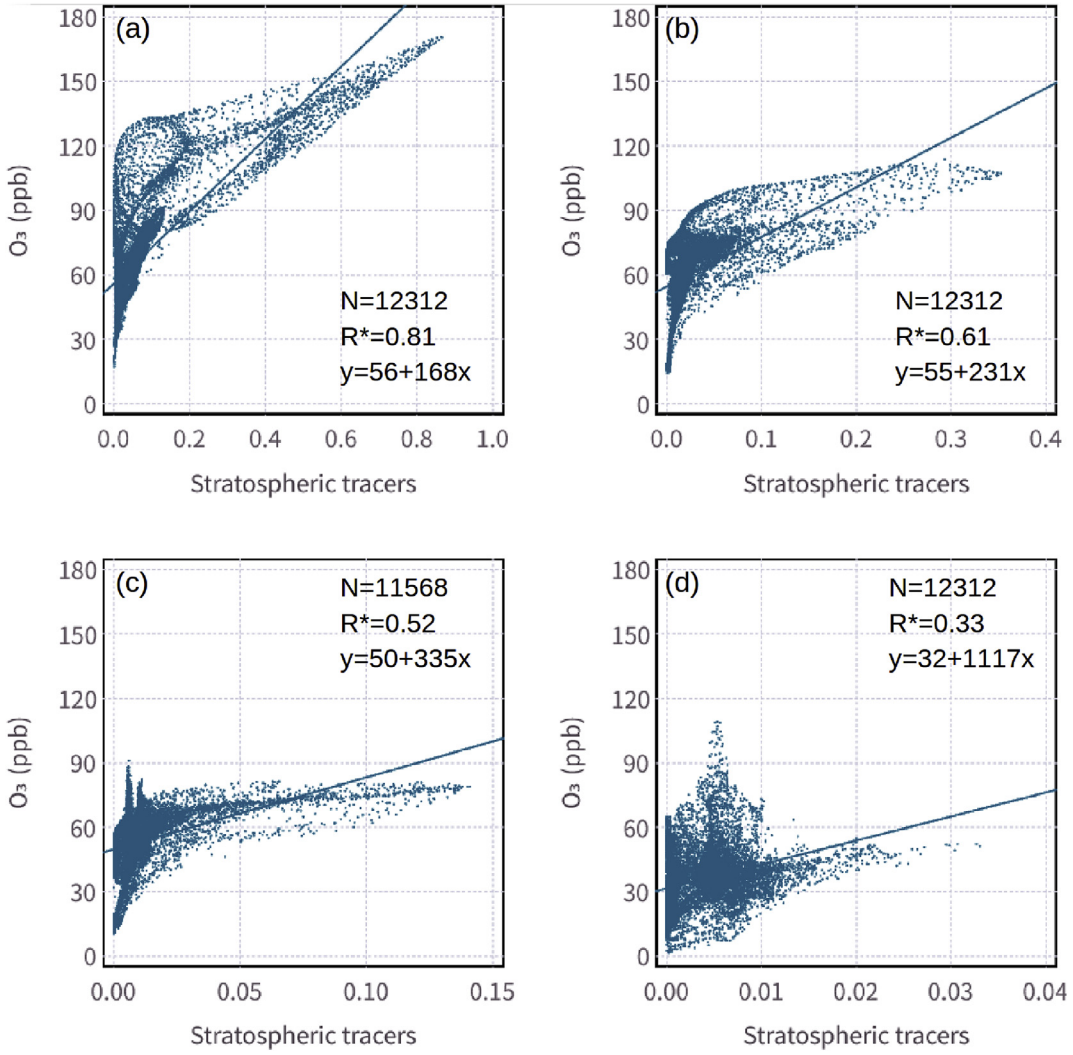


**Fig. 7.** Correlation between the simulated stratospheric tracers and $O_3$ concentration (ppb) in domain-grids, at (a) 300 hPa altitude, (b) 500 hPa altitude, (c) 700 hPa altitude and (d) surface, at 2:00 LST on August 29, 2016. (At the stratosphere, the passive tracer is set to a value of 1).

as shown in Fig. 8(b). Meanwhile, at the ground, it can be clearly seen that the spikes of high $O_3$ and simultaneously low CO as well as relative humidity (indicative of low water vapor) concurrently appeared from August 28 to 30, as indicated in Fig. 8(c), likely an effect of the stratospheric intrusion, in particular of considering the continuously high $O_3$ concentration (i.e., higher than 50 ppbv during the entire period including both day and night). This co-occurrence of low CO, low water vapor and abnormally nocturnal high $O_3$ concentration usually indicates that the $O_3$ pollution event was not related to local photochemical reactions but caused by the downward transport of the upper air (Wang et al., 2006). All these results confirm that the stratospheric source of $O_3$ had important contribution to the surface $O_3$ pollution over China during the 2016 Group of Twenty summit, which should be taken into account in making policy of control measures for $O_3$ in the future.

## 4. Conclusions

The effect of stratospheric intrusion on the near surface ozone concentration over eastern Asia during the campaign period of the 2016 G20 Summit was investigated with the WRF-Chem model in this study. Evaluation of model performance by using both the surface measurement and the OMI satellite retrievals shows that the WRF-Chem model was able to reasonably reproduced the ozone distributions in both the surface and the upper level. The modeling results demonstrate that the deepened tropopause fold appeared in the high-level curvature of upper-level jet streaks during the cyclogenesis, leading to stratosphere ozone intrusion. A fairly large number of passive stratospheric tracers, shaped as a “long-narrow belt”, was found in the low-troposphere (700-hPa altitude), showing the significant influence of stratosphere intrusion on ozone distribution. As a result, abnormally high $O_3$ and simultaneously low CO and relative humidity were also observed at the ground level. These results suggest that the stratospheric $O_3$ intrusion events have significant contribution to the local ground $O_3$ pollution, which is one of the reasons to explain the difficulty of $O_3$ control during the campaign period. Considering the cyclogenesis tends to become a climatological event in East Asia (Adachi and Kimura, 2007), more efforts on the frequency of stratospheric intrusion are required to investigate the elevated hemispheric $O_3$ in the future.

## Acknowledgements

This work was financially supported by the Ministry of Environmental Protection of China (No. 201409008-4), the Zhejiang Provincial Key Science and Technology Project for Social Development (No. 2014C03025), and the Natural Science Foundation of China (No. 51476144).

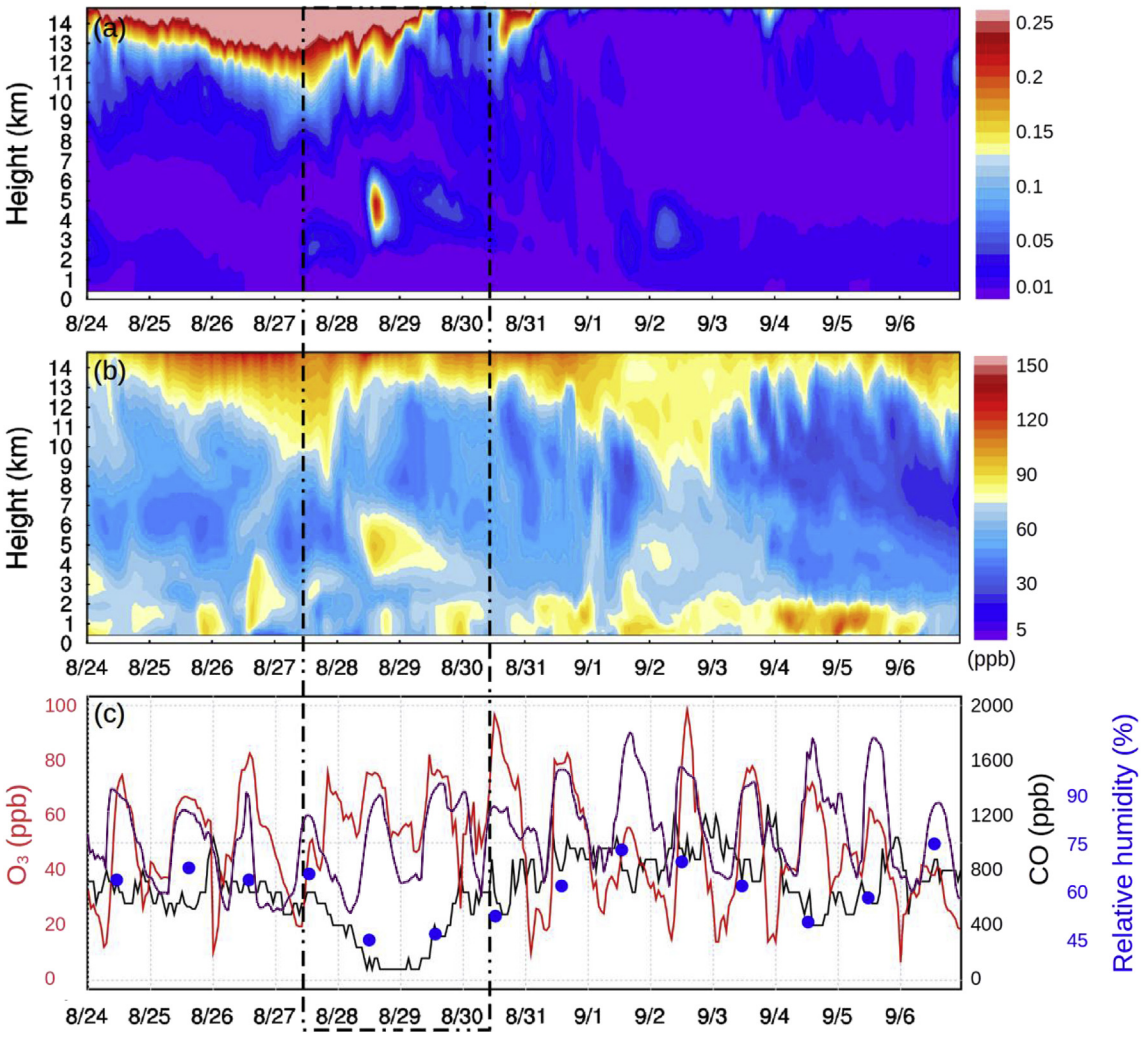


**Fig. 8.** Time series of hourly variations at the site of Jingdezhen (117.16°E, 29.26°N) during August 24–September 9, 2016. Modeled (a) stratospheric tracers (At the stratosphere, the passive tracer is set to a value of 1) and (b) $O_3$ concentration, and (c) surface concentrations of modeled $O_3$ (purple line; left axis), observed $O_3$ (red line; left axis), observed CO (black line; right black axis) and observed daily relative humidity (point; right blue axis). Dashed box indicates the stratospheric intrusion during the analyzed period.

## Appendix A. Supplementary data

Supplementary data to this article can be found online at https://doi.org/10.1016/j.apr.2019.02.010.

## References


Adachi, S., Kimura, F., 2007. A 36-year Climatology of Surface Cyclogenesis in East Asia Using High-resolution Reanalysis Data. Inside Solaris 3, 113–116. https://doi.org/10.2151/sola.2007-029.

Akritidis, D., Pozzer, A., Zanis, P., Tyrlis, E., Škerlak, B., Sprenger, M., Lelieveld, J., 2016. On the role of tropopause folds in summertime tropospheric ozone over the eastern Mediterranean and the Middle East. Atmos. Chem. Phys. 16, 14025–14039. https://doi.org/10.5194/acp-16-14025-2016.

Baklanov, A., Schlünzen, K., Suppan, P., Baldasano, J., Brunner, D., Aksoyoglu, S., Carmichael, G., Douros, J., Flemming, J., Forkel, R., Galmarini, S., Gauss, M., Grell, G., Hirtl, M., Joffre, S., Jorba, O., Kaas, E., Kaasik, M., Kallos, G., Kong, X., Korsholm, U., Kurganskiy, A., Kushta, J., Lohmann, U., Mahura, A., Manders-Groot, A., Maurizi, A., Moussiopoulos, N., Rao, S.T., Savage, N., Seigneur, C., Sokhi, R.S., Solazzo, E., Solomos, S., S??rensen, B., Tsegas, G., Vignati, E., Vogel, B., Zhang, Y., 2014. Online coupled regional meteorology chemistry models in Europe: Current status and prospects. Atmos. Chem. Phys. 14, 317–398. https://doi.org/10.5194/acp-14-317-2014.

Barth, M.C., Lee, J., Hodzic, A., Pfister, G., Skamarock, W.C., Worden, J., Wong, J., Noone, D., 2012. Thunderstorms and upper troposphere chemistry during the early stages of the 2006 North American Monsoon. Atmos. Chem. Phys. 12, 11003–11026. https://doi.org/10.5194/acp-12-11003-2012.

Boothe, A.C., Homeyer, C.R., 2017. Global large-scale stratosphere-troposphere exchange in modern reanalyses. Atmos. Chem. Phys. 17, 5537–5559. https://doi.org/10.5194/acp-17-5537-2017.

Bresky, W.C., Colucci, S.J., 1996. A forecast and analyzed cyclogenesis event diagnosed with potential vorticity. Mon. Weather Rev.

Brown, J.F., Loveland, T.R., Merchant, J.W., Reed, B.C., Ohlen, D.O., 1993. Using Multisource Data in Global Land-Cover Characterization - Concepts, Requirements, and Methods. Photogramm. Eng. Rem. Sens. 59, 977–987.

Calfapietra, C., Morani, A., Sgrigna, G., Di Giovanni, S., Muzzini, V., Pallozzi, E., Guidolotti, G., Nowak, D., Fares, S., 2016. Removal of Ozone by Urban and Peri-Urban Forests: Evidence from Laboratory, Field, and Modeling Approaches. J. Environ. Qual. 45, 224. https://doi.org/10.2134/jeq2015.01.0061.

Ding, A., Wang, T., 2006. Influence of stratopshere-to-troposhere exchange on the seasonal cycle of surface ozone at Mount Waliguan in western China. Geophys. Res. Lett. 33. https://doi.org/10.1029/2005GL024760.

Emmons, L.K., Walters, S., Hess, P.G., Lamarque, J.-F., Pfister, G.G., Fillmore, D., Granier, C., Guenther, A., Kinnison, D., Laepple, T., Orlando, J., Tie, X., Tyndall, G., Wiedinmyer, C., Baughcum, S.L., Kloster, S., 2010. Description and evaluation of the Model for Ozone and Related chemical Tracers, version 4 (MOZART-4). Geosci. Model Dev. 3, 43–67. https://doi.org/10.5194/gmd-3-43-2010.

Fadnavis, S., Beig, G., Buchunde, P., Ghude, S.D., Krishnamurti, T.N., 2011. Vertical transport of ozone and CO during super cyclones in the Bay of Bengal as detected by Tropospheric Emission Spectrometer. Environ. Sci. Pollut. Res. 18, 301–315. https://doi.org/10.1007/s11356-010-0374-3.

Fiore, A.M., Jacob, D.J., Bey, I., Yantosca, R.M., Field, B.D., Fusco, A.C., Wilkinson, J.G., 2002. Background ozone over the United States in summer: Origin, trend, and contribution to pollution episodes. J. Geophys. Res. Atmos. 107. https://doi.org/10.1029/2001JD000982.

Frey, W., Schofield, R., Hoor, P., Kunkel, D., Ravegnani, F., Ulanovsky, A., Viciani, S., D'Amato, F., Lane, T.P., 2015. The impact of overshooting deep convection on local transport and mixing in the tropical upper troposphere/lower stratosphere (UTLS). Atmos. Chem. Phys. 15, 6467–6486. https://doi.org/10.5194/acp-15-6467-2015.

Gauss, M., Isaksen, I.S.A., Lee, D.S., Søvde, O.A., 2006. Impact of aircraft $NO_x$ emissions on the atmosphere -tradeoffs to reduce the impact. Atmos. Chem. Phys. 6, 1529–1548. https://doi.org/10.5194/acp-6-1529-2006.

Greenslade, J.W., Alexander, S.P., Schofield, R., Fisher, J.A., Klekociuk, A.K., 2017. Stratospheric ozone intrusion events and their impacts on tropospheric ozone in the Southern Hemisphere. Atmos. Chem. Phys. 17, 10269–10290. https://doi.org/10.5194/acp-17-10269-2017.

Grell, G.A., Peckham, S.E., Schmitz, R., McKeen, S.A., Frost, G., Skamarock, W.C., Eder, B., 2005. Fully coupled "online" chemistry within the WRF model. Atmos. Environ. 39, 6957–6975. https://doi.org/10.1016/j.atmosenv.2005.04.027.

Guenther, a., Karl, T., Harley, P., Wiedinmyer, C., Palmer, P.I., Geron, C., 2006. Estimates of global terrestrial isoprene emissions using MEGAN (Model of Emissions of Gases and Aerosols from Nature). Atmos. Chem. Phys. 6, 3181–3210. https://doi.org/10.5194/acpd-6-107-2006.

Helmig, D., Oltmans, S.J., Morse, T.O., Dibb, J.E., 2007. What is causing high ozone at Summit, Greenland? Atmos. Environ. Times 41, 5031–5043. https://doi.org/10.1016/j.atmosenv.2006.05.084.

Holton, J.R., Haynes, P.H., McIntyre, M.E., Douglass, A.R., Rood, R.B., Pfister, L., 1995. Stratosphere-troposphere exchange. Rev. Geophys. https://doi.org/10.1029/95RG02097.

Hoskins, B., 2015. Potential vorticity and the PV perspective. Adv. Atmos. Sci. 32, 2–9. https://doi.org/10.1007/s00376-014-0007-8.

Hoskins, B., Pedder, M., Jones, D., 2003. The omega equation and potential vorticity. Q. J. R. Meteorol. Soc. 129, 3277–3303. https://doi.org/10.1256/qj.02.135.

Jaeglé, L., Wood, R., Wargan, K., 2017. Multiyear Composite View of Ozone Enhancements and Stratosphere-to-Troposphere Transport in Dry Intrusions of Northern Hemisphere Extratropical Cyclones. J. Geophys. Res. Atmos. 122 (13) 436-13,457. https://doi.org/10.1002/2017JD027656.

Keyser, D., Shapiro, M.A., 1986. A Review of the Structure and Dynamics of Upper-Level Frontal Zones. Mon. Weather Rev https://doi.org/10.1175/1520-0493(1986)114 < 0452:AROTSA > 2.0.CO;2.

Kheirbek, I., Wheeler, K., Walters, S., Kass, D., Matte, T., 2013. PM2.5 and ozone health impacts and disparities in New York City: Sensitivity to spatial and temporal resolution. Air Qual. Atmos. Heal. 6, 473–486. https://doi.org/10.1007/s11869-012-0185-4.

Landry, J.S., Neilson, E.T., Kurz, W.A., Percy, K.E., 2013. The impact of tropospheric ozone on landscape-level merchantable biomass and ecosystem carbon in Canadian forests. Eur. J. For. Res. 132, 71–81. https://doi.org/10.1007/s10342-012-0656-z.

Lefohn, A.S., Wernli, H., Shadwick, D., Limbach, S., Oltmans, S.J., Shapiro, M., 2011. The importance of stratospheric-tropospheric transport in affecting surface ozone concentrations in the western and northern tier of the United States. Atmos. Environ. 45, 4845–4857. https://doi.org/10.1016/j.atmosenv.2011.06.014.

Lelieveld, J., Hoor, P., Jöckel, P., Pozzer, A., Hadjinicolaou, P., Cammas, J.P., Beirle, S., 2009. Severe ozone air pollution in the Persian Gulf region. Atmos. Chem. Phys. 9, 1393–1406. https://doi.org/10.5194/acp-9-1393-2009.

Li, K., Chen, L., Ying, F., White, S.J., Jang, C., Wu, X., Gao, X., Hong, S., Shen, J., Azzi, M., Cen, K., 2017a. Meteorological and chemical impacts on ozone formation: A case study in Hangzhou, China. Atmos. Res. 196, 40–52. https://doi.org/10.1016/j.atmosres.2017.06.003.

Li, M., Zhang, Q., Kurokawa, J.-I., Woo, J.-H., He, K., Lu, Z., Ohara, T., Song, Y., Streets, D.G., Carmichael, G.R., Cheng, Y., Hong, C., Huo, H., Jiang, X., Kang, S., Liu, F., Su, H., Zheng, B., 2017b. MIX: a mosaic Asian anthropogenic emission inventory under the international collaboration framework of the MICS-Asia and HTAP. Atmos. Chem. Phys. 17, 935–963. https://doi.org/10.5194/acp-17-935-2017.

Lin, M., Fiore, A.M., Horowitz, L.W., Langford, A.O., Oltmans, S.J., Tarasick, D., Rieder, H.E., 2015. Climate variability modulates western US ozone air quality in spring via deep stratospheric intrusions. Nat. Commun. 6. https://doi.org/10.1038/ncomms8105.

Monks, P.S., Archibald, A.T., Colette, A., Cooper, O., Coyle, M., Derwent, R., Fowler, D., Granier, C., Law, K.S., Mills, G.E., Stevenson, D.S., Tarasova, O., Thouret, V., von Schneidemesser, E., Sommariva, R., Wild, O., Williams, M.L., 2015. Tropospheric ozone and its precursors from the urban to the global scale from air quality to short-lived climate forcer. Atmos. Chem. Phys. 15, 8889–8973. https://doi.org/10.5194/acp-15-8889-2015.

Morgan, M.C., Nielsen-Gammon, J.W., 1998. Using Tropopause Maps to Diagnose Midlatitude Weather Systems. Mon. Weather Rev. 126, 2555–2579 https://doi.org/10.1175/1520-0493(1998)126 < 2555:UTMTDM > 2.0.CO;2.

Ni, Z. zhen, Luo, K., Zhang, J. xi, Feng, R., Zheng, H. xin, Zhu, H. ran, Wang, J. fan, Fan, J. ren, Gao, X., Cen, K. fa, 2018. Assessment of winter air pollution episodes using long-range transport modeling in Hangzhou, China, during World Internet Conference, 2015. Environmental Pollution 550–561. https://doi.org/10.1016/j.envpol.2018.01.069.

Ojha, N., Pozzer, A., Akritidis, D., Lelieveld, J., 2017. Secondary ozone peaks in the troposphere over the Himalayas. Atmos. Chem. Phys. 17, 6743–6757. https://doi.org/10.5194/acp-17-6743-2017.

OMI team, 2012. Ozone monitoring instrument ( OMI ) data user ' s guide. In: Assessment.

Powers, J.G., Klemp, J.B., Skamarock, W.C., Davis, C.A., Dudhia, J., Gill, D.O., Coen, J.L., Gochis, D.J., Ahmadov, R., Peckham, S.E., Grell, G.A., Michalakes, J., Trahan, S., Benjamin, S.G., Alexander, C.R., Dimego, G.J., Wang, W., Schwartz, C.S., Romine, G.S., Liu, Z., Snyder, C., Chen, F., Barlage, M.J., Yu, W., Duda, M.G., 2017. The weather research and forecasting model: Overview, system efforts, and future directions. Bull. Am. Meteorol. Soc. 98, 1717–1737. https://doi:10.1175/BAMS-D-15-00308.1.

Royal Society, 2008. Ground-level ozone in the 21st century: future trends, impacts and policy implications. (October).

Sarangi, T., Naja, M., Ojha, N., Kumar, R., Lal, S., Venkataramani, S., Kumar, A., Sagar, R., Chandola, H.C., 2014. First simultaneous measurements of ozone, CO, and NOy at a high-altitude regional representative site in the central Himalayas. J. Geophys. Res. 119, 1592–1611. https://doi.org/10.1002/2013JD020631.

Schumann, U., Huntrieser, H., 2007. The global lightning-induced nitrogen oxides source. Atmos. Chem. Phys. Atmos. Chem. Phys. 7, 3823–3907. https://doi.org/10.5194/acpd-7-2623-2007.

Shankar Das, S., Venkat Ratnam, M., Narasimhan Uma, K., Venkata Subrahmanyam, K., Asatar Girach, I., Kumar Patra, A., Aneesh, S., Viswanathan Suneeth, K., Kishore Kumar, K., Parashuram Kesarkar, A., Sijikumar, S., Ramkumar, G., 2016. Influence of tropical cyclones on tropospheric ozone: Possible implications. Atmos. Chem. Phys. 16, 4837–4847. https://doi.org/10.5194/acp-16-4837-2016.

Shu, L., Xie, M., Wang, T., Gao, D., Chen, P., Han, Y., Li, S., Zhuang, B., Li, M., 2016. Integrated studies of a regional ozone pollution synthetically affected by subtropical high and typhoon system in the Yangtze River Delta region, China. Atmos. Chem. Phys. 16, 15801–15819. https://doi.org/10.5194/acp-16-15801-2016.

Stauffer, D.R., Seaman, N.L., Binkowski, F.S., 1991. Use of Four-Dimensional Data Assimilation in a Limited-Area Mesoscale Model Part II: Effects of Data Assimilation within the Planetary Boundary Layer. Mon. Weather Rev. 2 https://doi.org/10.1175/1520-0493(1991)119 < 0734:UOFDDA > 2.0.CO.

Stohl, A., Wernli, H., James, P., Bourqui, M., Forster, C., Liniger, M.A., Seibert, P., Sprenger, M., 2003. A new perspective of stratosphere-troposphere exchange. Bull. Am. Meteorol. Soc. 84 1565–1573 + 1473. https://doi.org/10.1175/BAMS-84-11-1565.

Su, W., Liu, C., Hu, Q., Fan, G., Xie, Z., Huang, X., Zhang, T., Chen, Z., Dong, Y., Ji, X., Liu, H., Wang, Z., Liu, J., 2017. Characterization of ozone in the lower troposphere during the 2016 G20 conference in Hangzhou. Sci. Rep. 7, 17368. https://doi.org/10.1038/s41598-017-17646-x.

Trickl, T., Vogelmann, H., Giehl, H., Scheel, H.E., Sprenger, M., Stohl, A., 2014. How stratospheric are deep stratospheric intrusions? Atmos. Chem. Phys. 14, 9941–9961. https://doi.org/10.5194/acp-14-9941-2014.

Tuccella, P., Curci, G., Visconti, G., Bessagnet, B., Menut, L., Park, R.J., 2012. Modeling of gas and aerosol with WRF/Chem over Europe: Evaluation and sensitivity study. J. Geophys. Res. Atmos. 117. https://doi.org/10.1029/2011JD016302.

U.S.EPA, 2007. Guidance on the Use of Models and Other Analyses for Demonstrating Attainment of Air Quality Goals for Ozone, PM2.5 and Regional Haze. USEPA.

Wang, S., Xing, J., Chatani, S., Hao, J., Klimont, Z., Cofala, J., Amann, M., 2011. Verification of anthropogenic emissions of China by satellite and ground observations. Atmos. Environ. 45, 6347–6358. https://doi.org/10.1016/j.atmosenv.2011.08.054.

Wang, T., Wong, H.L.A., Tang, J., Ding, A., Wu, W.S., Zhang, X.C., 2006. On the origin of surface ozone and reactive nitrogen observed at a remote mountain site in the northeastern Qinghai-Tibetan Plateau, western China. J. Geophys. Res. Atmos. 111. https://doi.org/10.1029/2005JD006527.

Wang, T., Xue, L., Brimblecombe, P., Lam, Y.F., Li, L., Zhang, L., 2017. Ozone pollution in China: A review of concentrations, meteorological influences, chemical precursors, and effects. Sci. Total Environ. 575, 1582–1596. https://doi.org/10.1016/j.scitotenv.2016.10.081.

Xie, M., Zhu, K., Wang, T., Yang, H., Zhuang, B., Li, S., Li, M., Zhu, X., Ouyang, Y., 2014. Application of photochemical indicators to evaluate ozone nonlinear chemistry and pollution control countermeasure in China. Atmos. Environ. 99, 466–473. https://doi.org/10.1016/j.atmosenv.2014.10.013.

Xue, L., Gu, R., Wang, T., Wang, X., Saunders, S., Blake, D., Louie, P.K.K., Luk, C.W.Y., Simpson, I., Xu, Z., Wang, Z., Gao, Y., Lee, S., Mellouki, A., Wang, W., 2016. Oxidative capacity and radical chemistry in the polluted atmosphere of Hong Kong and Pearl River Delta region: Analysis of a severe photochemical smog episode. Atmos. Chem. Phys. 16, 9891–9903. https://doi.org/10.5194/acp-16-9891-2016.

Xue, L.K., Wang, T., Gao, J., Ding, A.J., Zhou, X.H., Blake, D.R., Wang, X.F., Saunders, S.M., Fan, S.J., Zuo, H.C., Zhang, Q.Z., Wang, W.X., 2014. Ground-level ozone in four Chinese cities: Precursors, regional transport and heterogeneous processes. Atmos. Chem. Phys. 14, 13175–13188. https://doi.org/10.5194/acp-14-13175-2014.

Yang, Q., Cunnold, D.M., Choi, Y., Wang, Y., Nam, J., Wang, H.-J., Froidevaux, L., Thompson, A.M., Bhartia, P.K., 2010. A study of tropospheric ozone column enhancements over North America using satellite data and a global chemical transport model. J. Geophys. Res. 115, D08302. https://doi.org/10.1029/2009JD012616.

Zhang, Y., Zhang, X., Wang, L., Zhang, Q., Duan, F., He, K., 2016. Application of WRF/Chem over East Asia: Part I. Model evaluation and intercomparison with MM5/CMAQ. Atmos. Environ. 124, 285–300. https://doi.org/10.1016/j.atmosenv.2015.07.022.